ELSEVIER

Polymer 43 (2002) 1323–1330

polymer

www.elsevier.com/locate/polymer

# X-ray diffraction and computational studies of the modulus of silk (*Bombyx mori*)

A. Sinsawat[a], S. Putthanarat[a], Y. Magoshi[b], R. Pachter[c], R.K. Eby[a,*]

[a]*Department of Polymer Science, The University of Akron, Akron, OH 44325-3909, USA*
[b]*National Institute of Sericultural and Entomological Science-CREST, Tsukuba 305, Japan*
[c]*AFRL/MLPJ, WPAFB, Dayton, OH 45433-7702, USA*

Received 30 July 2001; received in revised form 3 October 2001; accepted 5 October 2001

**Abstract**

X-ray diffraction with the assumption of uniform stress has been used for determining the crystal modulus of polymers. Values of the modulus of silk obtained previously using such an approach were found to be an order of magnitude lower than, those obtained by computational modeling. The differences are outside the limits of experimental and computational errors. This study re-examined the values in an improved manner. For the X-ray technique, moduli of different samples along the length of cocoon fibers were measured. The values obtained are 20–28 GPa depending on the crystallinity index and degree of orientation of the samples. For the computational calculation, the longitudinal acoustic mode (LAM) frequency of silk systems having three different *c*-axis dimensions were calculated. An acoustic dispersion curve was generated from the frequency values. The slope of the curve at the origin gave a crystal modulus of 13 GPa. A 3D-fluctuation analysis yielded an average modulus of approximately 16 GPa. These low values result from the out-of-plane torsioning of molecules in the β-pleated structure of the silk crystals. The experimental and computational results are in reasonable agreement with one another as well as with data reported in the literature for other pleated molecules. 

*Keywords*: Longitudinal acoustic dispersion curve; 3D-fluctuations; Molecular dynamics

## 1. Introduction

Mechanical properties of bulk polymers are governed in a complicated manner by many factors, such as the connectivity of the various phases, the orientation, size and distribution of the crystallites as well as the molecular mobility of the chains. Thus, by studying the close relationship between the structure and mechanical properties of polymers both theoretically and experimentally, one should be able to obtain a better understanding of the complicated behavior of the mechanical properties of polymers. One disadvantage of synthetic high performance fibers is that their compressive strength is much smaller than their tensile strength [1]. Those fibers generally buckle under much lower compressive loads than does silk. The factor contributing to such a property might be the fact that the fibers of silk are not solid but are made up of nanofibrils [2,3]. The small diameter of these structures increases the flexibility of the fiber and decreases the maximum tensile and compressive stresses at the surface of a bent fiber in comparison with the corresponding values for a solid fiber [4]. The crystal modulus also plays a role in determining these quantities. In some published articles, there is approximately an order of magnitude difference between the calculated and the experimental values of crystal modulus [3,5–7]. The difference between those values obtained from the two different approaches appears to be outside the limits of error and probably represents some conceptual error. Therefore, both the experimental and computational values have been redetermined in an improved manner in the present work. This includes making measurements on samples with differing crystallinities and orientations as determined by X-ray diffraction. For the computational approach, the β-pleated conformation of $(\text{glycine–alanine})_n$ was used together with molecular dynamics (MD).

## 2. Experimental investigation

### 2.1. Sample preparation

Seven cocoons of *Bombyx mori* silk were reeled simultaneously from a hot water bath (95–100 °C) and separated into samples every 112 m. Even though the degree of

* Corresponding author. Tel.: +1-330-972-5397; fax: +1-330-972-6581.
*E-mail address:* eby@polymer.uakron.edu (R.K. Eby).

0032-3861/02/$ - see front matter 
PII: S0032-3861(01)00696-6

crystallite orientation does not change when the fibers are stretched as much as possible [5], extra care was taken to minimize any additional strain on the fibers during reeling. Twelve samples were obtained and degummed as reported earlier [4]. Samples 1 and 12 represent fiber obtained from the outermost and innermost regions of the cocoons, respectively. One hundred small lengths were cut from each sample and bundled together (1400 fibers). These bundles were mounted in sample holders using epoxy.

### 2.2. Instrumentation

The X-ray detector system used in these measurements was a 2D-detector HISTAR model with general area detector diffraction systems (GADDS) software, which runs on Windows NT. The X-ray generator was a Rigaku–Denki RU-200 rotating anode. The voltage and current of the generator were set at 50 kV and 150 mA, respectively. The radiation was from a copper target. A nickel filter was used to limit the radiation primarily to the Cu Kα wavelength of 1.5418 Å. The X-ray beam was collimated using a 0.3 mm Siemens pinhole collimator. The X-ray diffraction patterns were obtained in a helium environment in order to reduce the background scattering correction. The sample to detector distance was set at 7.30 cm with silicon.

### 2.3. Evaluation of crystal modulus

With the X-ray measurements, the crystallinity index and degree of orientation for the different samples were evaluated. This was followed by the determination of crystal modulus using the assumption of uniform stress distribution. According to the assumption, crystal modulus can be evaluated from the relationship between the macroscopic (applied) stress and the crystal strain. A method similar to that reported previously was used [6]. The crystal strain was evaluated from the change of the *d*-spacing of the reflecting plane that has its normal along the molecular axis. This plane is observed through the meridional (002) reflection. The maximum strain used was about 0.012. During the crystal modulus measurements, samples were tilted by the (002) Bragg angle towards the incident beam in order to obtain a stronger (002) reflection from planes perpendicular to the fiber axis. Load was gradually applied to the sample by a method of increasing strain. This approach eliminated the effect of rapidly increasing the stress and the associated risk of breaking the sample while adding a dead weight. The stress was calculated as load divided by the cross sectional area of the bundle of fibers as determined from the length, mass and density of the bundle. The stress relaxation of the sample after the initial application of strain was compensated for by a further increase in the applied strain before X-ray measurements were made. The method yielded values of the modulus with an estimated uncertainty of about ±0.6 GPa.

## 3. Computational investigation

### 3.1. Simulation details

The computations were performed using the Insight II 400P + commercial software. The process was started with the generation of a repeated sequence of glycine and alanine. This repeated sequence was used as a simplified model for the crystal structure of *B. mori* silk [8–10]. The torsional angles of this chain were adjusted to obtained the β-pleated conformation. The energy of the chain was minimized to relieve energetic strain while keeping the torsional angles fixed. Once a minimized chain was obtained, three molecular models each consisting of 16 molecules of $(gly–ala)_n$ were generated. The three assemblies differed in the number, *n*, of glycine–alanine repeated sequences, with *n* being 8, 10, and 15. The CVFF force field was used throughout the calculations because it was designed to reproduce protein properties. Cross terms were included except during the early refinement of the unit cell. In this force field, the hydrogen bonds are a natural consequence of the standard van der Waals and electrostatic parameters. The non-bonded interactions were calculated using group-based cutoffs. These interactions were truncated at 14 Å with a spline width of 10 Å [11] to avoid discontinuities in the energies at the cutoff. A buffer width of 0.5 Å, which provides the inclusion of neighboring atoms while calculating the non-bonded interactions, was also used.

To obtain an equilibrated structure, MD simulations were carried out under constant pressure dynamics (NPT). The temperature of the system was brought up from the minimum energy temperature to 300 K with increments of 50 K. The duration of simulation for each increment was 1 ps. The pressure of the system was controlled using the Parrinello–Rahman method. This method allowed both cell size and shape to change. The temperature was controlled using Anderson's method. The equations of motion were integrated using the Verlet velocity integrator with a time step of 1 fs. The equilibration process at 300 K was carried out for 400 ps. This was followed by a data collection period of 600 ps. The peak to peak strain of the fluctuations along the molecular axis was about 0.012.

### 3.2. Calculation of crystal modulus

By assuming that the system behaves as an elastic rod, the longitudinal acoustic mode (LAM) frequency in wave number ($\bar{u}$) obtained from the MD simulations could be used to calculate the crystal modulus with the following expression [12]:

$$\bar{u} = \left(\frac{m}{2cL}\right)\left(\frac{E}{\rho}\right)^{1/2} \quad (1)$$

where *c* is the velocity of light, *L* the length of the molecular chain, *E* the modulus, ρ the density of the system, and *m* is an integer equal to 1.

Another approach, which can be used to calculate the modulus, is the 3D-fluctuation analysis. The basis of this technique is the thermal motion, which causes the system of atoms to move, leading to changes in various system parameters (e.g. spatial continuation vectors which describe the geometry of the system [13]). These vectors have small-amplitude fluctuations about their mean values and can be used to evaluate the strain tensor $\epsilon$. According to Parrinello–Rahman, the strain tensor can be used to calculate the stiffness matrix ($C_{ij}$) [13,14]

$$C_{ij} = \frac{kT}{V}\langle \epsilon_i \epsilon_j \rangle^{-1} \quad (2)$$

The term $V$ represents the mean volume of the system, $k$ the Boltzmann constant, and $T$ is the temperature.

## 4. Results and discussion

### 4.1. X-ray diffraction

For a sample with large perfectly oriented crystals, the diffraction pattern would consist of an array of very small spots. For silk fibers, these spots are smeared into broadened arcs as a result of the small crystal size and imperfect orientation of crystals (Fig. 1a). Three crystalline peaks and one amorphous peak were used to fit the intensity profile along the equatorial direction. The reflections due to the crystalline regions were indexed as (100), (200), and (120) [15]. The choice of a proper baseline is important in analyzing the diffraction pattern. A linear baseline was chosen and found to be sufficient for the observed data. The crystallinity index was evaluated from the equatorial reflections within the $2\theta$ range of 5–30° [5,16,17]. Since all the crystalline and amorphous reflections could not be measured because of instrumental limitations, the term 'crystallinity index' is used rather than 'crystallinity'. The degree of orientation was evaluated from the half width at half maximum (HWHM) of the intensity profile along the azimuthal direction of the equatorial 200 reflection.

In general, the intensity due to the amorphous scattering must be separated from that due to crystalline diffraction. However, the lack of an amorphous template of silk led to some difficulty in subtracting the amorphous scattering. The small misalignment of each of the individual fibers in the bundles further complicated the evaluation of the orientation. It caused the peaks to broaden and led to a decrease of orientation. In the present measurements, the crystallinity index and degree of orientation both increased as fibers towards the inner portion of the cocoons were measured (Figs. 2 and 3). This behavior might result if the silk fibroin crystallizes to form fibers with better crystallinity and orientation from a changed solution present at the end of the fiber spinning process. It might also be possible that the fibers produced later in the spinning process are subjected to more tensile stress during the formation of the cocoon. The unit cell dimensions remained nearly unchanged with position along the fibers, as did the crystal dimension perpendicular to the (200) plane.

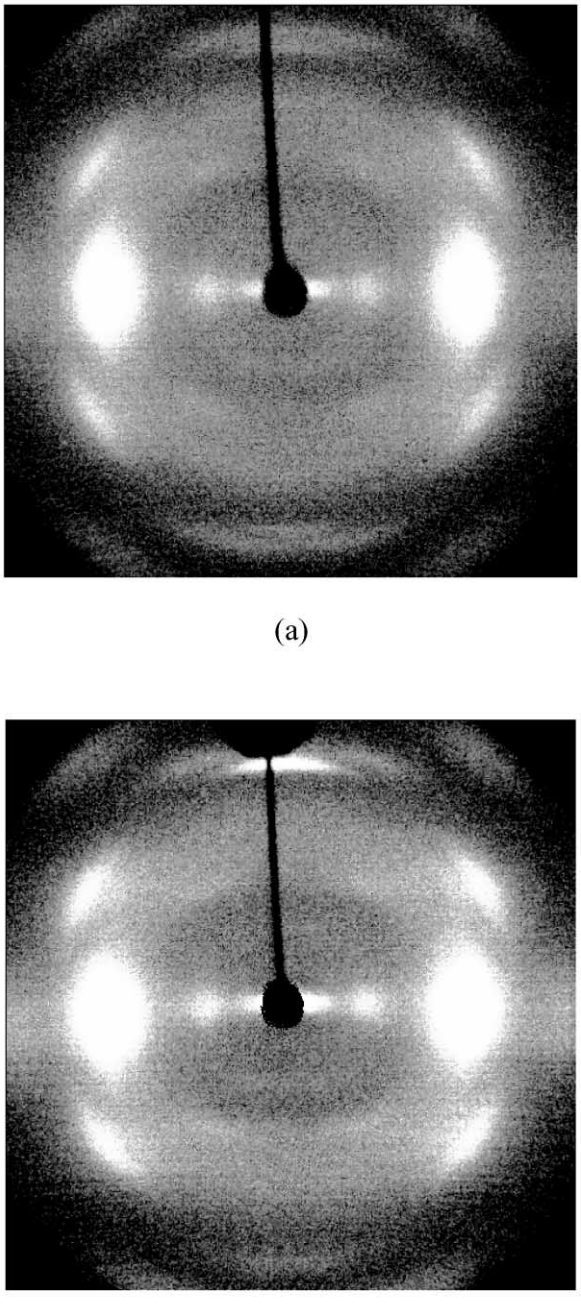


Fig. 1. X-ray fiber patterns of silk fibers obtained when the fibers: (a) were aligned perpendicular to and (b) were aligned with their top tilted towards the incident beam.

Tilting the samples by the Bragg angle for the (002) planes resulted in two major advantages during the crystal modulus measurement. First, more of the meridional (002) spot in reciprocal space was brought into coincidence with the sphere of reflection. The intensity of this peak increased

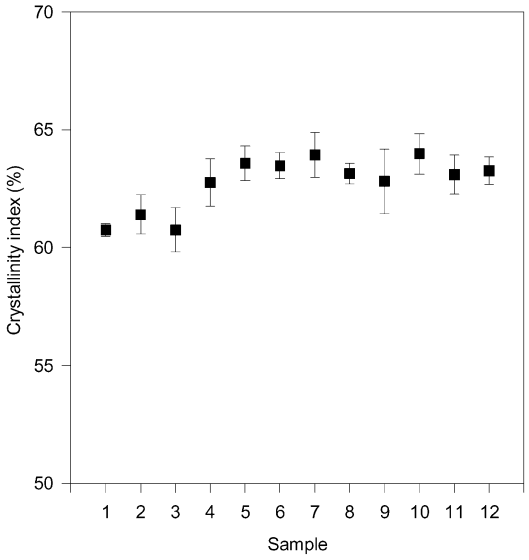


Fig. 2. Evaluation of crystallinity index from equatorial reflections obtained with fibers along the length of the cocoon of *B. mori*. The error bars shown represent the standard deviation of repeated measurements.

(top of Fig. 1b) leading to a better observation of the peak shift as a result of the applied load. Second, by tilting the sample, the change of the *d*-spacing of the (002) peak observed from the X-ray diffraction pattern is a result of stress directly applied to the sample (along *A*) and not from a reduced stress on planes at − and + the Bragg angle (along *B* and *C*) to the applied stress for an untilted sample (Fig. 4).

In general a semi-crystalline polymer is treated in terms of a mixture of two phases: perfect crystal and ideal amorphous. The simplest composite arrangements of the two phases are in parallel and in series. These result in uniform strain and uniform stress, respectively, on the

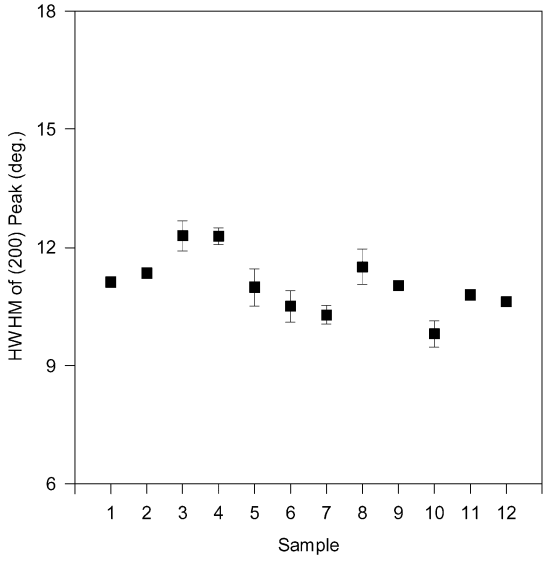


Fig. 3. Evaluation of orientation from the equatorial (200) reflection obtained from fibers along the length of the cocoon of *B. mori*. The error bars shown represent the standard deviation of repeated measurements.

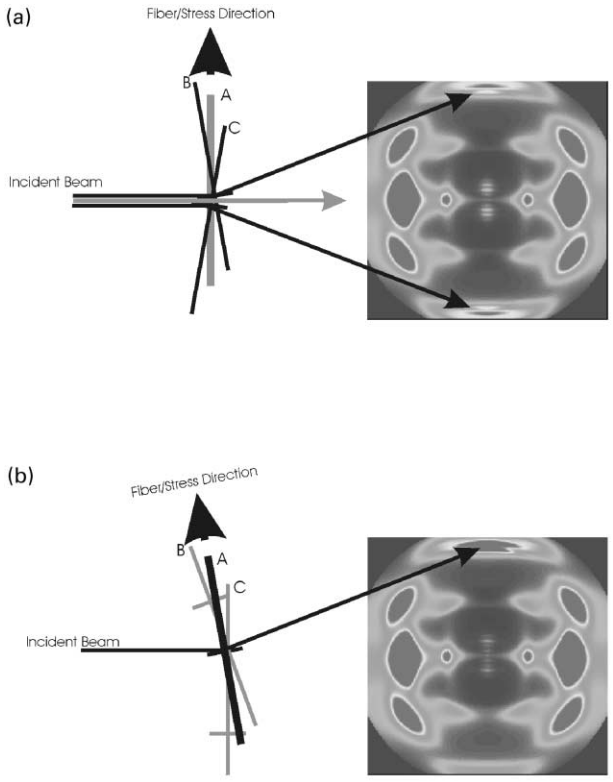


Fig. 4. Simulated diffraction patterns for samples: (a) aligned perpendicular to and (b) tilted by the Bragg angle for the (002) planes towards the incident beam. Line A is parallel to the fiber axis. Lines B and C are in the plane defined by the beam and line A, but at − and + the Bragg angle from A, respectively. In (a), they are black to indicate that the (002) planes perpendicular to them contribute strongly to the 002 diffraction and line A is grey to indicate a weaker contribution. In (b), the fiber is rotated by − the Bragg angle. Planes perpendicular to A (black) contribute strongly and those perpendicular to B and C (grey) contribute weakly.

crystals. Of the two, uniform stress has been argued to give a better estimation of the crystal modulus along molecular axis direction. So far, there has not been agreement on the validity of the uniform stress assumption. The basic argument supporting the uniform stress assumption is that it gave consistent values for the crystal modulus when samples with differing bulk modulus were used [18]. However, the properties also will depend on the arrangement and connectivity of these two very different phases as well as on their amount and orientation. The arrangement of these phases controls how the stress is distributed within the material and hence the modulus. Any imperfection in the orientation of the crystals reduces the modulus of the fibers. In addition, X-ray data used for the determination of the crystal modulus obtained from the fiber bundles was subject to some uncertainties, as the orientation of fibers in a bundle and the mechanical loads on them cannot be made completely uniform. The application of stress had the effect of bringing about a partial reorientation as well as a deformation of the crystals. These problems could be reduced by using synchrotron radiation and a smaller bundle of fibers. The present measurements show that the crystal modulus

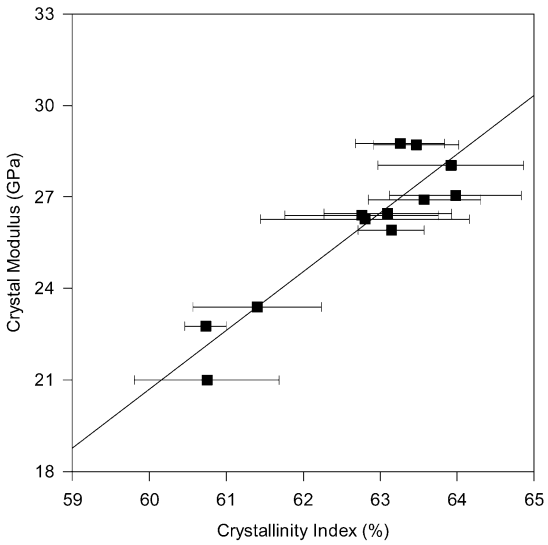


Fig. 5. Variation of crystallinity index and crystal modulus of fibers along the length of the cocoon of *B. mori*. The error bars shown represent the standard deviation of repeated measurements.

increased as the crystallinity index and orientation of the fibers increased as fibers towards the inner portion of the cocoon were measured (Figs. 5 and 6). The fact that crystal moduli vary with the crystallinity index and orientation further suggests the deficiency of the uniform stress assumption. Some analytical and empirical analyses of the variation of crystal modulus with crystallinity and orientation have been reported [19–21]. However, the problems cannot be removed completely without much more knowledge of the fine structure.

### 4.2. Computation

The energy-minimized structure has a density of $1.355 \pm 0.004$ g/cm$^3$, which is comparable to the values reported earlier [22]. The calculated *d*-spacings agree reasonably well with those major reflections observed in X-ray measurements (Table 1).

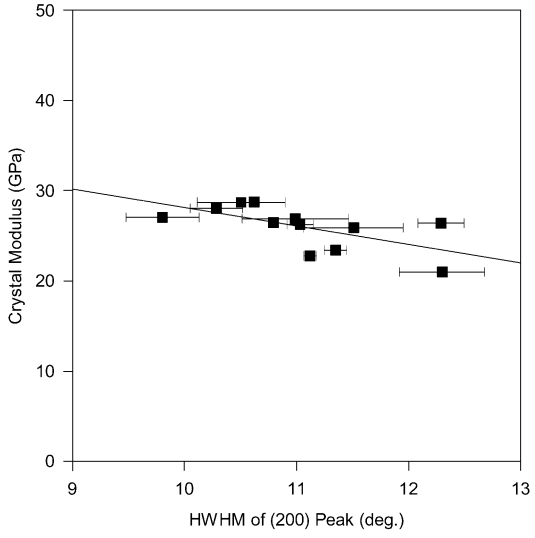


Fig. 6. Variation of degree of orientation and crystal modulus of fibers along the length of the cocoon of *B. mori*. The error bars shown represent the standard deviation of repeated measurements.

Starting from this minimized structure, MD simulation was performed. Once the simulation was completed, the fluctuation of the length along the molecular axis direction as a function of the simulation time was Fourier transformed. This process converted the 'time domain' representation of the deformation to the 'frequency domain' (Fig. 7).

As illustrated in Ref. [26], the LAM frequency was taken to be the dominant peak in the low frequency region (e.g. near $0.0009 \times 10^{14}$ Hz in Fig. 7). The three systems with different numbers of *c*-axis repeats yielded three different frequencies. They are components of the longitudinal acoustic dispersion curve. These frequencies could, in principle, be used to evaluate the modulus according to Eq. (1). This equation can be rearranged as follows:

$$\nu = \frac{1}{2l\pi}\left(\frac{m\pi}{n}\right)\left(\frac{E}{\rho}\right)^{1/2} \tag{3}$$

where $\nu$ is the calculated frequency, $l$ the length of the repeat unit, and $n$ is number of the repeat units. The frequencies calculated from the three different simulated systems were plotted as a function of the phase angle $m\pi/n$. The curve was fitted with an exponential function (Fig. 8). The numbers of *c*-axis repeats used in the calculation are quite small and did not produce frequencies in the 'linear' region as implied by the relationship between frequency and phase angle in Eq. 3 [12]. As illustrated earlier, the modulus cannot be calculated from such frequencies using the uniform elastic rod model for short chains (small $n$) [12]. Despite the non-linearity of the curve, the crystal modulus could be calculated from the slope at the origin. This calculation yields a modulus of 13 GPa with a statistical uncertainty of about 2%. Fitting with a cubic or a quadratic function yields different but similar numbers.

The stiffness matrix ($C_{ij}$) of silk obtained from the 3D-fluctuation analysis is shown below. The values in the lighter type are expected to be zero for an orthorhombic system. The deviations from zero value could indicate

Table 1
Comparisons of observed and calculated *d*-spacings of three major reflections for crystals of the silk of *B. mori*

| Reflections | *d*-spacing (Å) | | | |
|---|---|---|---|---|
| | This work | | Reported | Reference |
| | Observed | Calculated | | |
| (100) | 9.70 | 9.70 | 9.70 | [10,23,24] |
| (200) | 4.66 | 4.46 | 4.68 | [15] |
| | | | 4.70 | [10] |
| | | | 4.48 | [25] |
| (002) | 3.48 | 3.48 | 3.53 | [9] |
| | | | 3.48 | [10,15] |

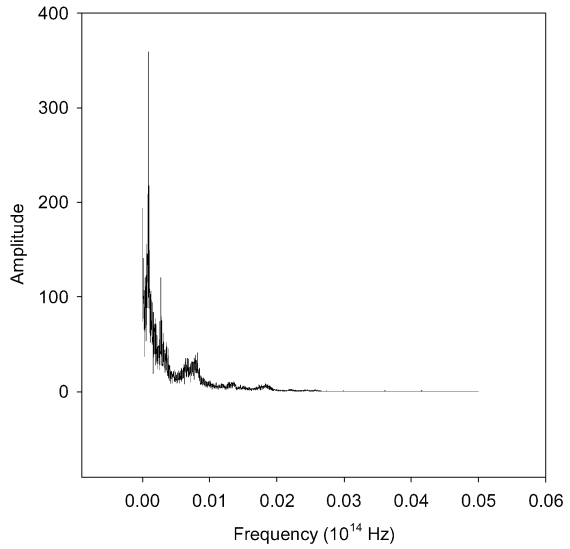


Fig. 7. Frequency domain representation of the fluctuation of the simulated system with ten glycine–alanine sequences along the molecular axis direction.

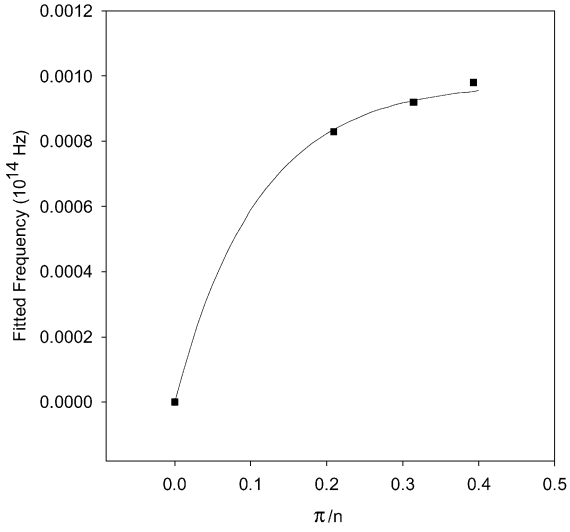


Fig. 8. Longitudinal acoustic dispersion curve for $m = 1$. The frequency values were obtained from the MD simulations.

deviation from the orthorhombic symmetry as an inherent consequence of the constant pressure dynamics as well as other uncertainties in the results. The formation of the hydrogen bonds between adjacent chains results in a large value of stiffness ($C_{11}$) along their direction. Such large values of transverse stiffness have also been observed in other polymers with strong inter-molecular coupling [27–29]. In addition, the effect of the hydrogen bonds together with the inter-sheet inter-digitation of the other side groups can contribute to the shear constants $C_{44}$, $C_{55}$ and $C_{66}$ which are a little larger than those for, say, polyethylene [13]

$$\begin{pmatrix} \mathbf{38} & \mathbf{7} & \mathbf{11} & -0.4 & 0.1 & 0.3 \\ \mathbf{7} & \mathbf{19} & \mathbf{19} & 0.0 & -0.1 & -0.4 \\ \mathbf{11} & \mathbf{19} & \mathbf{37} & -0.3 & -0.5 & 0.5 \\ -0.4 & 0.0 & -0.3 & \mathbf{7} & 0.2 & 0.1 \\ 0.1 & -0.1 & -0.5 & 0.2 & \mathbf{7} & 0.0 \\ 0.3 & -0.4 & 0.5 & 0.1 & 0.0 & \mathbf{4} \end{pmatrix}$$

In general, the simulations almost always result in $C_{ij}$ values that depend largely on the duration of the dynamic runs at shorter times. Hence, it is difficult to specify the extent to which the calculated elastic constants are reliable. To estimate the accuracy of the results, the stiffness and compliance along the chain direction, $C_{33}$ and $S_{33}$, were plotted against the number of averaging molecular dynamic steps (Fig. 9). From the plot, it was reasonable to conclude that the results did not change with simulation time for the time-scale used.

To obtain the crystal modulus ($E_{33}$), the compliance matrix ($S_{ij}$) had to be calculated by inverting the $C_{ij}$ matrix. The values of the latter have been estimated to be subjected to a statistical uncertainty of approximately 10% [13]. The compliance along the molecular axis at different numbers of averaging molecular dynamic steps is also depicted in Fig. 9b. From the compliance matrix, the Young's modulus along the chain direction or the crystal modulus was

Table 2
Comparisons between the crystal modulus values of silk and other polymers

| Materials | Reference | Crystal modulus (GPa) | | Structural contraction (%) |
|---|---|---|---|---|
| | | Computational | Experimental | |
| Silk (extended) | [5] | 150 | – | 0 |
| Silk (β-pleated) | | 13, 16 | 20–28 | 6 |
| Nylon 6 α-form extended) | [32–34] | 244, 263, 312 | 183 | 0 |
| Nylon 6 γ-form (pleated) | [36] | 54 | 21 | 3 |
| Poly-L-glycine I (extended) | [7] | 147 | – | 0 |
| Poly-L-glycine II (pleated) | [35] | 12 | – | – |
| Poly-L-alanine (extended) | [36] | 160 | – | 0 |
| Poly-L-alanine (α-helical) | [36] | 60 | – | 53 |
| Poly-L-alanine (β-pleated) | [6,37] | – | 16–17, 20 | 4 |

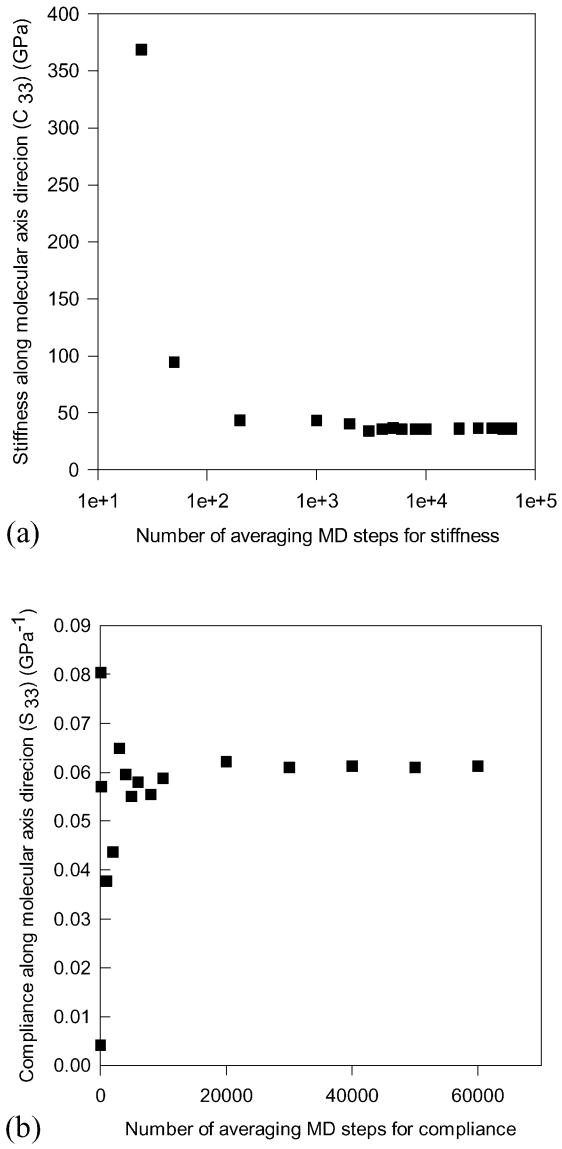


Fig. 9. Stiffness ($C_{33}$) : (a) and compliance ($S_{33}$) (b) along the chain direction of silk crystals as a function of the number of averaging molecular dynamic steps for the ten repeat units sequences.

calculated as $E_{33} = 1/S_{33}$. The three simulated systems yielded slightly different results with an average modulus of 16 GPa. Analyzing the fluctuations in the values of $S_{33}$ of the last six points for all the three simulated systems indicated a statistical uncertainty of about 8% in the values of $E_{33}$. The difference between the calculated values and those obtained from X-ray measurement might be the result of the absence of serine in the computational model. This represents approximately 12% of the amino acids in the crystalline regions. This serine group has an –OH side chain, which is capable of forming hydrogen bonds. The higher modulus of the actual silk sample could originate from the role of such hydrogen bonds. Other factors might introduce errors in all the experimental results. These include the unknown arrangement and connectivity of the different phases present. Also, the structural relaxation and the associated stress relaxation, which occur during the time period of the X-ray measurements, could affect the applied stress and hence the results. An improvement would be to reduce this effect by making the measurement at a synchrotron, which would reduce the measurement time.

It has been extensively investigated and shown that crystal modulus depends on such factors as conformation, cross-sectional area per molecule, and molecular packing [18,30,31]. Among these factors, the structural conformation seems to be the dominant one. The force required to distort a bond increases as the distortion changes from bond rotation to bond bending and stretching. For polymers with contracted conformations, e.g. silk in the β-pleated crystal, the majority of the force applied to the molecules would result in the torsional deformation of the bonds. Hence, the modulus along the molecular axis direction of such polymers is much smaller than that for molecules with an extended conformation for which the deformation involves solely bending and stretching of the covalent bonds. It has been shown for other molecules that the crystal modulus reduces to approximately 10–20% of the original value for the planar zigzag chain for a contraction of about 3% in length (Table 2). (Note that the modulus of α-helical poly-L-alanine is increased by hydrogen bonds along the molecule.) The low crystal modulus values for silk obtained from the present computations, which are comparable to those obtained from the X-ray measurement, emphasize the importance of this factor. More importantly, the moduli obtained by both methods are comparable to those of other polymers with a similar skeletal conformation (Table 2).

## 5. Conclusions

For the X-ray measurement, tilting the sample by the Bragg angle led to a more accurate determination of crystal stress and strain, which consequently resulted in a better evaluation of crystal modulus. From this measurement, it was observed that the crystal modulus values varied among fiber samples with differing crystallinity index and degree of orientation between the outer and inner portions of the cocoon. The unknown internal connectivity among crystalline and amorphous regions makes the exact interpretation of the X-ray data difficult. The structural and associated stress relaxations that occur during the measurements add to the difficulty. This and other problems could be reduced by using synchrotron radiation. The measurements of crystallinity index and orientation should be improved. By using the β-pleated structural conformation as the molecular model of silk, the computational crystal moduli obtained were in qualitative agreement with the values obtained from the X-ray measurement and with the moduli of other polymers with similarly contracted conformations. It is possible that the absence of serine in the computational

model contributes to the difference between X-ray and computational two results.

## Acknowledgements

The authors thank the Wright–Patterson Air Force Research Laboratories for supporting this research. They also thank Professor Gregory Rutledge of MIT, Dr Bruno Fanconi of NIST and Dr Bruce Eichinger of Accelrys for very helpful discussions and suggestions. Finally, they thank the reviewers for valuable suggestions and comments.

## References

[1] Jiang H, Adams WW, Eby RK. In: Cahn RW, Haasen P, Kramer EJ, editors. High performance polymer fibers: material science and technology (A comprehensive treatment), vol. 12. New York: VCH, 1993. Chapter 13.
[2] Putthanarat S, Eby RK, Adams WW, Liu GF. JMS-Pure Appl Chem 1996;A33(7):899.
[3] Mahoney DL, Vezie DL, Eby RK, Adams WW, Kaplan DL. In: Kaplan DL, Adams WW, Farmer BL, Viney C, editors. Silk polymers: materials science and biotechnology, ACS symposium series 544. Washington, DC: American Chemical Society, 1994. Chapter 18.
[4] Putthanarat S, Stribeck N, Fossey SA, Eby RK, Adams WW. Polymer 2000;41:3487.
[5] Iizuka E. Biorheology 1965;3:1.
[6] Becker MA, Mahoney DV, Lenhert PG, Eby RK, Kaplan D, Adams WW. In: Kaplan DL, Adams WW, Farmer BL, Viney C, editors. Silk polymers: materials science and biotechnology, ACS symposium series 544. Washington, DC: American Chemical Society, 1994. Chapter 17.
[7] Fanconi B. J Chem Phys 1972;57:2109.
[8] Oka M. Polym J 1990;22:416.
[9] Fossey SA, Nemethy G, Gibson KD, Scheraga HA. Biopolymer 1991;31:1529.
[10] Marsh RE, Corey RB, Pauling L. Biochim Biophys Acta 1955;16:1.
[11] Patniak SS, Pachter R. Polymer 1999;40:6507.
[12] Rabolt JF. Crit Rev Solid State Mater Sci 1985;12:165.
[13] Gusev AA, Zehnder MM, Suter UW. Macromol Symp 1995;90:85.
[14] Parrinello M, Rahman A. J Chem Phys 1982;76:2662.
[15] Warwicker JO. J Mol Biol 1960;2:350.
[16] Grubb DT, Jelinski LW. Macromolecules 1997;30:2860.
[17] Iizuka E. J Seric Sci Jpn 1996;65:102.
[18] Sakurada I, Ito T, Nakamae K. J Polym Sci C 1966;15:75.
[19] Brew B, Clements J, Davies GR, Jakeways R, Ward IM. J Polym Sci Polym Phys Ed 1979;17:351.
[20] Jiang H, Eby RK, Adams WW, Lenhert J. The materials science and engineering of rigid rod polymers. In: Adams WW, Eby RK, McLemore D, editors. MRS Symposium Proceedings. vol. 134. Pittsburgh, PA: Materials Research Society, 1989. p. 341.
[21] Jiang H. PhD dissertation, Johns Hopkins University, 1989.
[22] Ishikawa H. In: Hojo N, editor. Zoku kenshi no kozo (structure of silk proteins). Nagano: Shinkyo, 1980. p. 209.
[23] Iizuka E, Sawasa K, Motojima K. J Seric Sci Jpn 1998;67:217.
[24] Somashekar R, Gopalkrishna UR, Madhava MS. J Appl Polym Sci 1992;44:2161.
[25] Fraser RDB, MacRae TP. Conformation in fibrous proteins and related synthetic polypeptides. New York: Academic Press, 1973. Chapter 13.
[26] Macturk KS, Eby RK. Polymer 1994;35:55.
[27] Nicholson TM, Unwin AP, Ward IM, Siripittayananon J, Wongchanapiboon T. J Chem Soc, Faraday Trans 1995;91:2623.
[28] Sakata Y, Unwin AP, Nicholson TM, Ward IM. Comput Theor Polym Sci 1997;7:175.
[29] Urbanek S, Tashiro K, Kitayama T, Hatada K. Polymer 1999;40:3345.
[30] Sun Z, Morgan RJ, Lewis DN. Polymer 1992;33:725.
[31] Rutledge GC, Suter UW. Polymer 1991;32:2179.
[32] Manley TR, Martin CG. Polymer 1973;14:632.
[33] Tashiro K, Tadokoro H. Macromolecules 1981;14:781.
[34] Kaji K, Sakurada I. Macromol Chem 1978;179:209.
[35] Fanconi B. Biopolymers 1973;12:2759.
[36] Adams WW, Pachter R, Haaland PD, Horn TR, Wierschke SG, Crane R. Mater Res Soc Symp 1993;305:39.
[37] Nishino T, Nakamae K, Takahashi Y. Polymer 1992;33:1328.